

Dielectric Assist Accelerating Structures for Compact Linear Accelerators of Low Energy Particles in Hadrontherapy Treatments

Pablo Martinez-Reviriego^{†,1}, Daniel Esperante^{1,2}, Alexej Grudiev³, Benito Gimeno¹, César Blanch¹, Daniel González-Iglesias¹, Nuria Fuster-Martínez¹, Pablo Martín-Luna¹, Eduardo Martínez¹, Abraham Menendez¹ and Juan Fuster¹

¹Instituto de Fisica Corpuscular (CSIC - University of Valencia), [62980] Paterna, Spain

²also at Department of Electronic Engineering - ETSE, [46100] Burjassot, Spain

³CERN, [1217] Meyrin, Switzerland

Abstract—Dielectric Assist Accelerating (DAA) structures based on ultralow-loss ceramic are being studied as an alternative to conventional disk-loaded copper cavities. This accelerating structure consists of dielectric disks with irises arranged periodically in metallic structures working under the $TM_{02-\pi}$ mode. In this paper, the numerical design of an S-band DAA structure for low beta particles, such as protons or carbon ions used for Hadrontherapy treatments, is shown. Four dielectric materials with different permittivity and loss tangent are studied as well as different particle velocities. Through optimization, a design that concentrates most of the RF power in the vacuum space near the beam axis is obtained, leading to a significant reduction of power loss on the metallic walls. This allows to fabricate cavities with an extremely high quality factor, over 100 000, and shunt impedance over 300 M Ω /m at room temperature. During the numerical study, the design optimization has been improved by adjusting some of the cell parameters in order to both increase the shunt impedance and reduce the peak electric field in certain locations of the cavity, which can lead to instabilities in its normal functioning.

Index Terms—Dielectric assist accelerating (DAA) structures, radio frequency (RF), linac, Hadrontherapy, standing wave.

I. INTRODUCTION

OVER many years, room-temperature disk-loaded copper radio frequency (RF) structures have been deeply studied and implemented in a wide range of applications, for fundamental science [1] to cancer therapy [2] and industrial activities [3]. However, one of the main challenges of RF cavities for accelerators consists in achieving high accelerating gradient. The Compact Linear Collider (CLIC) project [4] was able to reach 100 MV/m gradient for X-band normal conducting copper structures. This High Gradient (HG) technology is currently being transferred from linear colliders to different fields of application such as compact linear accelerators for Hadrontherapy treatments [5]–[7]. Nevertheless, room temperature RF cavities are substantially less efficient than superconducting structures regarding power consumption, despite being able to reach higher gradients. An encouraging alternative to conventional disk-loaded copper structures is a dielectric loaded accelerating (DLA) structure [8]–[10].

A DLA structure consists of a dielectric tube surrounded by a conducting cylinder. The dielectric decreases the phase velocity as well as the ratio of the peak electric field to the average accelerating gradient, which is about unity [11], [12]. In dielectric breakdown studies, a surface field threshold of 13.8 GV/m was observed at THz frequencies [13], and no breakdowns have been observed in several high-power tests carried out on DLA structure at a level >5 MW. However, one of the drawbacks of dielectric structures is multipactor discharge [14]–[17]. Thus, the main issues limiting the performance of DLA structures are surface multipactor and RF breakdowns due to strong local field enhancement in micro-scale vacuum gap in the dielectric joint [18], [19].

The concept of DLA structure was proposed in the 1940's [20]–[23], and first experimental measurements were carried out in the 1950s [24]–[26]. However, disk-loaded metallic structures were more successful in that time due to their high quality factor and field holding capabilities. Recently, thanks to a remarkable progress in new ceramic materials with high dielectric permittivity ($\epsilon_r > 20$), low loss ($\tan \delta < 10^{-4}$) [27]–[29], and ultra-low loss ($\tan \delta < 10^{-5}$) [30]–[32], DLA structures are again being studied for multiple applications such as dual-layered DLA structure [33], a hybrid dielectric and iris-loaded accelerating structure [34], and a dielectric disk accelerating (DDA) structure [35]. Some examples of these dielectrics are fused silica, chemical vapor deposition (CVD) diamond or alumina, among other ceramics, some of which have been experimentally tested with high-power wakefield at Argonne National Laboratory [36], [37].

Based on these technologies, a Dielectric Assist Accelerating (DAA) structure proposed by Satoh *et al.* [38]–[40] at C-band frequency is of particular interest since it achieved extremely high quality factor and shunt impedance. Later, this design was studied at X-band as a proposal for future linear accelerators [41] due to its high field holding capability. Building on these developments, a DAA structure for low beta particles operating at low frequency (S-band) is studied for the first time in this work, as a solution for compact linear accelerators of low energy and low beam current, such as medical accelerators for Hadrontherapy treatments.

[†] pablo.martinez.reviriego@ific.uv.es

This paper shows a numerical study of an efficient S-band DAA structure operating under the $TM_{02-\pi}$ accelerating mode for four different dielectrics (CVD Diamond, MgO, $MgTiO_3$, $BaTiO_x$) and different particle velocities ($\beta = v/c = \{0.4, 0.5, \dots, 1\}$), where c is the speed of light in vacuum. This mode allows to reduce power loss on the conducting wall, achieving very high quality factor Q_0 , and shunt impedance Z_{eff} , at room temperature if the right dielectric material is chosen. A comparison with high-gradient copper-disk loaded structure for compact linear accelerators for medical use is shown.

II. GEOMETRY OPTIMIZATION

On the contrary to conventional disk-loaded copper structures, that operate in a TM_{01} mode and achieve high Z_{eff}/Q_0 , DAA structures operate under a TM_{02} mode in order to reduce the surface field and increase the quality factor. The dielectric allows to decrease the size of the structure and concentrate the electromagnetic energy near the beam axis, which consequently reduces copper losses and increases the shunt impedance. Thus, it is crucial that the dielectrics cost low power loss, show good thermal conductivity and withstand high electromagnetic fields.

The DAA structures [38], [41] consist of axially symmetric dielectric cylinders with irises periodically arranged in a metallic enclosure operating in standing wave π -mode, as illustrated in Fig. 1.

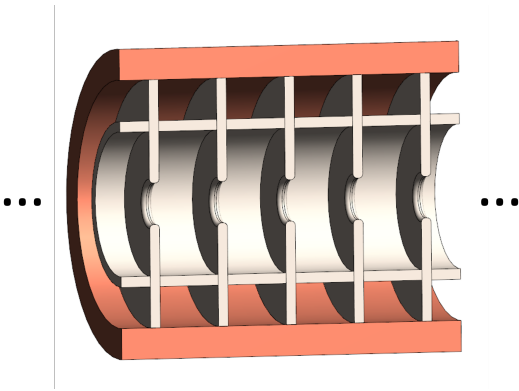


Fig. 1. Conceptual schematic of an infinite S-band DAA structure.

A. Regular cell design

DAA design starts by optimizing parameters for the regular cell in order to maximize the Q_0 and the Z_{eff} for the resonant frequency of interest. The longitudinal cross section of the regular cell can be seen in Fig. 2, where r_0 is the aperture radius, r_c is the corner filet radius, a_1 is the inner radius, b_1 is the outer radius, c_1 is the copper waveguide radius, d_1 is the dielectric disk thickness, also known as iris, and L_1 is the constant periodic length.

Once L_1 , r_0 and r_c are selected based on criteria explained later, the combination of a_1 , b_1 , c_1 and d_1 determines the figures of merit in the cavity, such as resonant frequency, quality factor and shunt impedance of the accelerating mode

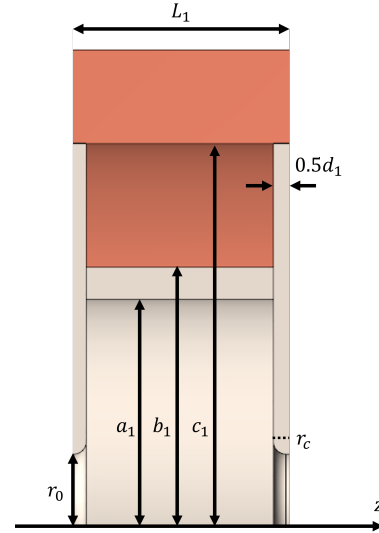


Fig. 2. Longitudinal cross section geometry of a regular cell of a DAA accelerator structure.

$TM_{02-\pi}$. Thus, in this paper a new step is added to the optimization analysis, looking for the value of d_1 which, in combination with the three radius selection, maximizes the shunt impedance of the cavity, in spite of fixing this value to $d_1 = \lambda_0/(4\sqrt{\epsilon_r})$ as was done in previous studies [38], [41]. Thanks to the axial symmetry, optimum parameters can be calculated using the SUPERFISH tool [42], in addition results have been cross checked using HFSS [43]. Periodic boundary conditions were applied to regular cell in order to simulate an infinite long structure.

The resonant frequency goal was fixed at $f_0 = (3000 \pm 2)$ MHz, $L_1 = \beta\lambda_0/2$, where $\lambda_0 = c/f_0$ is the free space wavelength, $r_0 = 2$ mm for comparison with high gradient copper structures and $r_c = d_1/2$. Then, in order to find the best values for d_1 and the radii a_1, b_1, c_1 , a two step scan needs to be done. First, d_1 is fixed at its initial value $d_1 = d_0 = \lambda_0/(4\sqrt{\epsilon_r})$, so the resonant frequency f_0 is determined by the combination of a_1 , b_1 and c_1 . Once a_1 and c_1 are fixed, the value of b_1 can be recalculated for the given frequency f_0 using the numerical solver. Following this methodology, optimum parameters can be found by sweeping through a_1 and c_1 , finding the corresponding value of b_1 , Q_0 and Z_{eff}/Q_0 . This is shown in Fig. 3 for $MgTiO_3$ with $\epsilon_r = 16.66$ and $\tan \delta = 0$. It must be noted here that for low electric permittivity and low particle velocity, it might be impossible to find a geometry of a regular cell with the desired resonant frequency.

This process is repeated for each value of a second swept in $d_1 = \xi d_0$, where ξ is the normalized iris thickness. This allows to find a better solution in terms of Z_{eff} , as illustrated in Fig. 4 for $MgTiO_3$ with $\epsilon_r = 16.66$ and $\tan \delta = 3.43 \times 10^{-5}$.

The ratio of the peak electric field E_p and the peak magnetic field H_p to the average accelerating electric field E_a usually limit the achievable accelerating gradient for conventional iris-loaded metallic structures, where

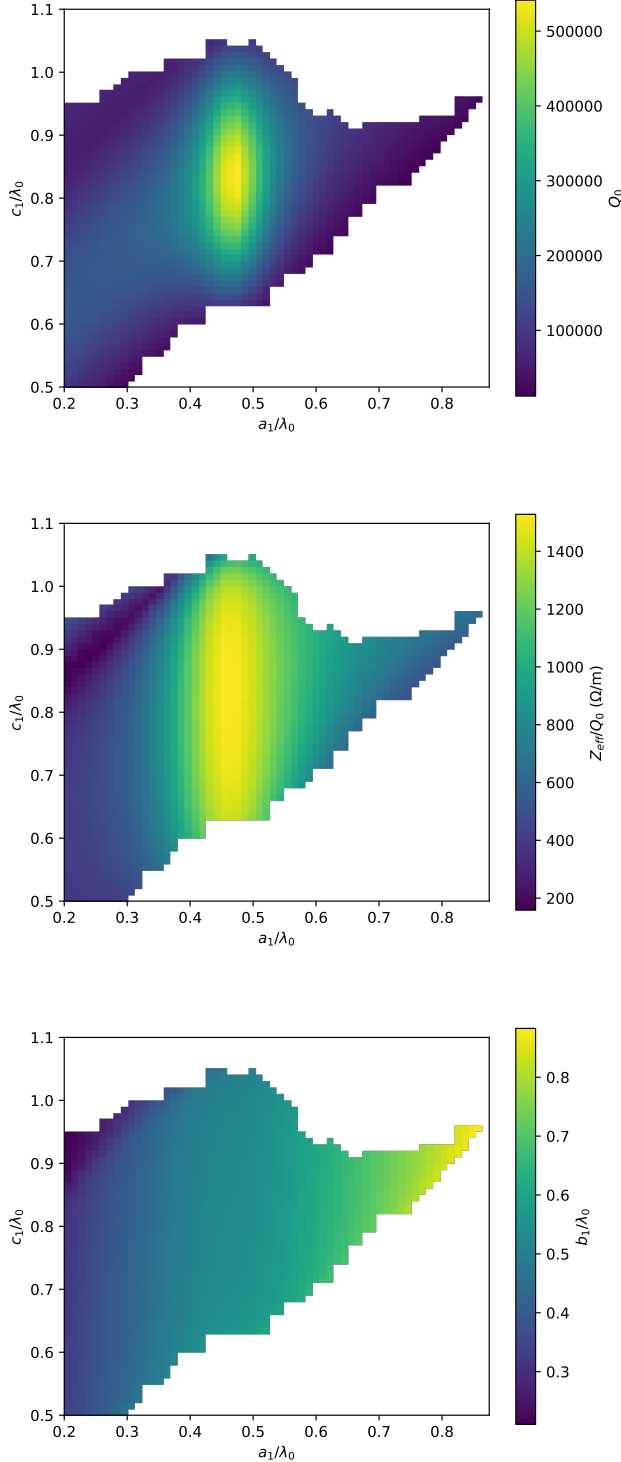


Fig. 3. Numerical unloaded quality factor Q_0 , shunt impedance over quality factor Z_{eff}/Q_0 and geometric parameter b_1 as a function of geometrical parameters a_1 and c_1 for a regular cell using ideal dielectric MgTiO_3 and $\beta = 0.6$. White region is due to the absence of a valid solution for the geometry.

$$E_a = \frac{1}{L_1} \int_{-L_1/2}^{L_1/2} E_z(0, 0, z) \cos\left(\omega \frac{z}{\beta c}\right) dz, \quad (1)$$

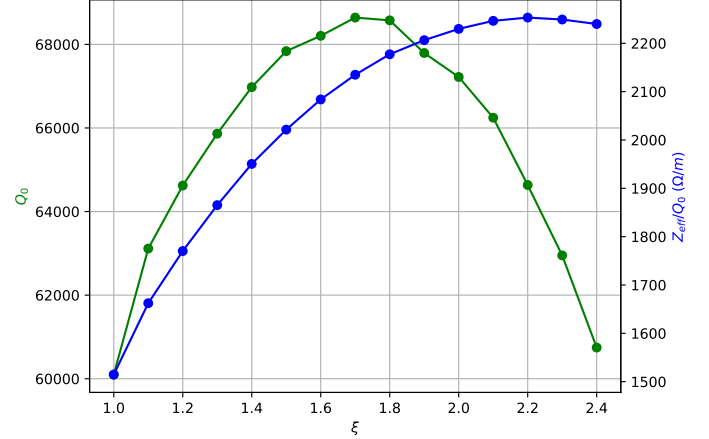


Fig. 4. Numerical unloaded quality factor Q_0 and shunt impedance over quality factor Z_{eff}/Q_0 as a function of normalized iris thickness for a regular cell using real dielectric MgTiO_3 and $\beta = 0.6$.

where E_z is the longitudinal component of the electric field, $\omega = 2\pi f$ is the angular frequency and z is the longitudinal spatial coordinate. Field profiles for this structure are illustrated in Fig. 5.

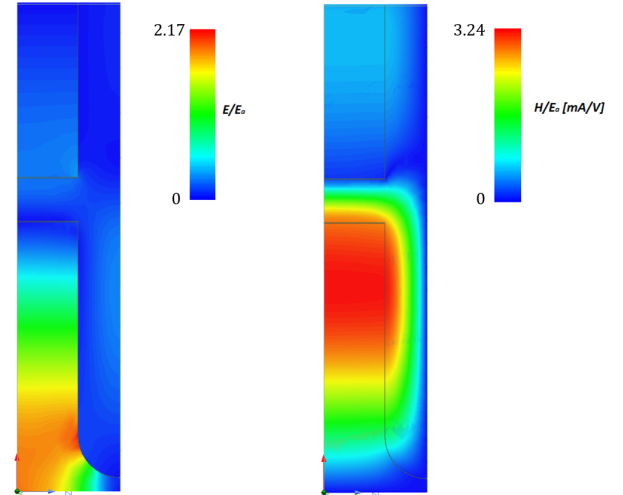


Fig. 5. Electric field distribution E/E_a and magnetic field distribution H/E_a for the accelerating mode $\text{TM}_{02-\pi}$ in a half regular cell using MgTiO_3 , $\beta = 0.6$ and $\xi = 2$.

an optimization was done using four different ceramics, whose electromagnetic properties can be found in Table I, and particles velocity $\beta = \{0.4, 0.5, 0.6, 0.7, 0.8, 0.9, 1\}$. During these studies, it was observed that the geometry optimization depends mainly on the particle velocity β and the relative electric permittivity ϵ_r of the ceramic, while loss tangent $\tan \delta$ determines the final value of Q_0 as well as Z_{eff} .

Energy ranges for Hadrontherapy treatments vary between 70-230 MeV for protons and 100-430 MeV/u for carbon ions, which correspond to particle velocities between 0.37-0.60 and 0.43-0.73, respectively [44]. Final results for the figures of

TABLE I
LIST OF DIELECTRICS STUDIED IN THE OPTIMIZATION

Material	Acronym	ϵ_r	$\tan \delta$
CVD Diamond	Diamond	5.7	3×10^{-6}
MgO	D9	9.64	6×10^{-6}
MgTiO ₃	D16	16.66	3.43×10^{-5}
BaTiO _x	D50	50.14	8×10^{-5}

merit for these designs, taking into account dielectric losses, are compared with an extension for all particle velocities of a high-gradient standing wave copper cavity designed for protons with $\beta = 0.38$ [45], as it can be seen in Fig. 6.

Note the difference on the performance between the ideal and relativistic case. For the ideal case, the Q_0 is over two orders of magnitude higher compared to HG copper structures. As can be seen in Fig. 6, the Q_0 increases with ϵ_r and it is very sensitive to losses in the dielectric, though results are better than normal copper cavities. One caveat of this design is that a high amount of electrical energy is stored inside the dielectric, which is not going to be used to accelerate the beam. As a consequence, energy efficiency worsens, resulting in lower values of Z_{eff}/Q_0 . Energy efficiency improves for larger ϵ_r and, as expected, does not depend on the dielectric $\tan \delta$. The performance of the structure will be given by the shunt impedance, which is a compromise between Q_0 and Z_{eff}/Q_0 . For the ideal case, the final result will be better for higher ϵ_r . However, due to the high sensitivity of Q_0 with dielectric losses, the characteristic value of $\tan \delta$ of the material is crucial on the real performance of the final structure. In addition, the performance increases also for higher particle velocities.

Moreover, as it is shown in Fig. 7, E_p/E_a for the optimal geometry decreases with the material permittivity and particle velocity and it is always below 4 which is the value obtained for CCL-HG cavity [45]. This ratio is one of the main limiting factors for HG cavities, since it is related with breakdowns production. Besides, it was observed that this ratio also decreases for thinner irises. Therefore, the performance of the DAA regular cell improves with particle velocity and higher electric permittivity being able to improve current values for room-temperature copper cavities.

B. Dielectric loss tangent

The advantage of working under the $TM_{02}-\pi$ mode, is that metallic losses are highly suppressed and, consequently, the DAA regular cell performance will be determined mainly by the quality of the dielectric in terms of its $\tan \delta$.

Dielectric and metallic losses are given by [38],

$$P_d = \frac{1}{2} \omega \epsilon_0 \epsilon_r \tan \delta \int_V |\mathbf{E}|^2 d\tau, \quad (2)$$

$$P_c = \frac{1}{2} R_s \int |\hat{\mathbf{n}} \times \mathbf{H}|^2 dS, \quad (3)$$

respectively, where $R_s = \sqrt{\omega \mu_0 / (2\sigma)}$ is the surface resistance, $\epsilon_0 \epsilon_r$ is the electric permittivity of dielectric, \mathbf{E} is the electric field, \mathbf{H} is the magnetic field, $\hat{\mathbf{n}}$ is the unitary

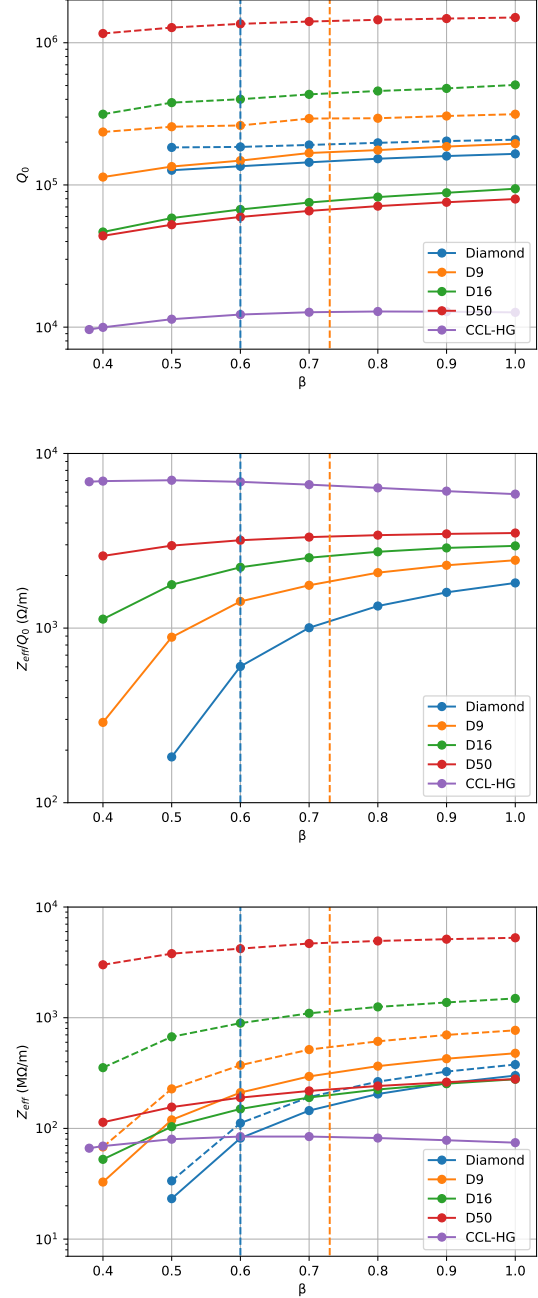


Fig. 6. Final results for Q_0 , Z_{eff}/Q_0 and Z_{eff} for the different values of particle velocity and different material in the ideal case (dashed lines), and taking into account dielectric losses (solid lines). Vertical dashed lines correspond to the maximum energy of protons (blue) and carbon ions (orange). The results are compared with a high-gradient cell coupled linac CCL-HG copper cavity (purple line) [45].

normal vector to the surface, μ_0 is the magnetic permeability of vacuum and $\sigma = 5.8 \times 10^7$ S/m is the copper electric conductivity.

A graphical representation of both surface and volumetric loss densities are illustrated in Fig. 8. As both magnitudes have different units, a quantitatively comparison between them must be done by integrating the loss density over the whole

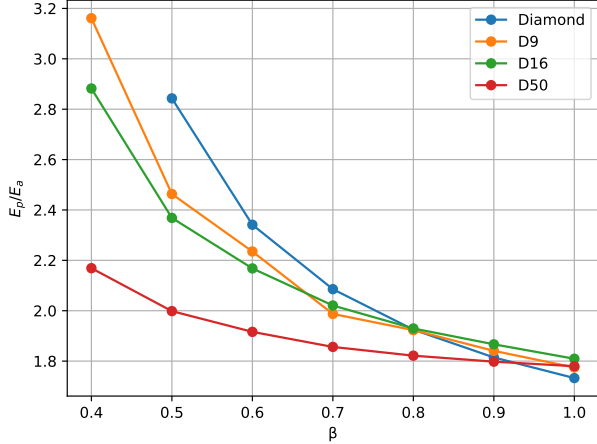


Fig. 7. Ratio of peak electric field and average accelerating field for different materials and particle velocities.

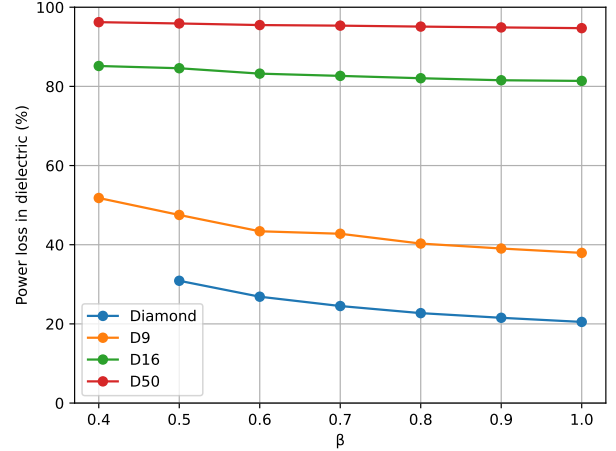


Fig. 9. Percentage of losses in the dielectric for different material and particle velocities.

geometry. Results are illustrated in Fig. 9, showing a strong dependence mainly on the material loss tangent.

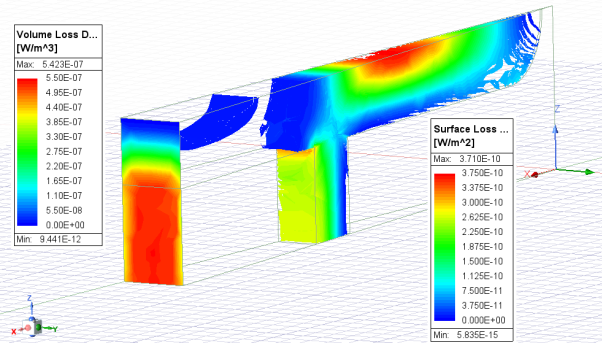


Fig. 8. Surface metallic and volumetric dielectric losses density for accelerating mode $TM_{02-\pi}$ in a regular cell using $MgTiO_3$, $\beta = 0.6$, stored electromagnetic energy $W = 1$ J and $\xi = 2$.

As the loss tangent depends strongly on the manufacturing process for the ceramic fabrication, values of Table I are just references from previous experimental measurements. Therefore, it is of great importance to study the dependence of regular cell performance as a function of the $\tan \delta$ of the material, as illustrated in Fig. 10, where an exponential decrease of the cavity performance can be seen for values of $\tan \delta > 10^{-5}$.

III. STRUCTURE PERFORMANCE

Once the optimization of the geometry has been performed, the electromagnetic performance of the regular cell has to be considered as a component of a real accelerator system. In order to do so, the dispersion relation of the regular cell is studied as well as the field instabilities and singularities which can lead to multipactor or RF breakdown discharges. Besides, the consequences of using coating to suppress multipactor in the RF performance is also deliberated.

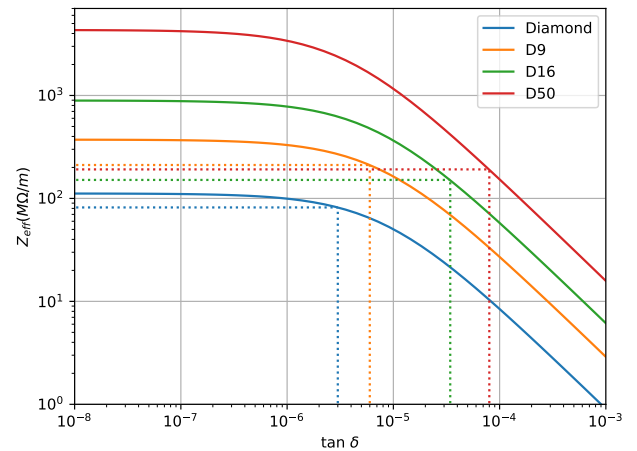


Fig. 10. Shunt impedance as a function of $\tan \delta$ for different materials and $\beta = 0.6$. Experimental $\tan \delta$ values for each material are shown.

A. Dispersion relation

The overlapping between adjacent modes is a typical problem from the tunability and operational point of view for periodic RF accelerating structures, which is the case for the standing-wave accelerating structure studied in this work. In addition, good electromagnetic coupling between consecutive cells is also a key factor in order to determine the maximum number of cells per cavity.

Electric coupling between consecutive cells improves for lower electric permittivity and particle velocity, as it is illustrated in Fig. 11. It can be observed that the TM_{02} mode is strongly electrically coupled, so there is no need for coupling cells between regular cells.

Dispersion curves for the second order mode and the next higher order mode are depicted in Fig. 12 for each material for two different normalized iris thickness. It can be seen that

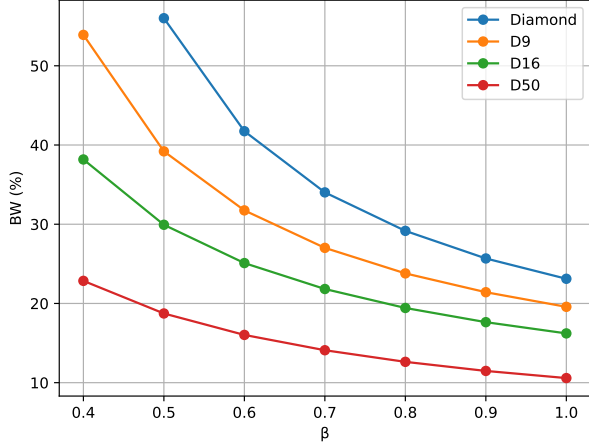


Fig. 11. Electrical coupling bandwidth for different materials and particle velocities with normalized iris thickness $\xi = 1.5$. The bandwidth is defined as $BW = (f_\pi - f_0)/f_\pi \cdot 100\%$.

for low electric permittivity material, the higher order mode crosses the 3 GHz point and, therefore, overlapping cannot be avoided. In addition, as the iris becomes thicker, it can be seen that higher order modes with a phase advance of π get closer to the resonant frequency and they can even cross this point for thicker irises. Consequently, electric permittivity and normalized iris thickness are bounded by the overlapping process.

B. Field instabilities

The existence of sharp angles and triple junction points in the original design can lead to singularities in the surface electric field. As a consequence, field instabilities, RF breakdowns or multipactor discharges can emerge.

Regarding the triple junction point (point B in Fig. 13), assuming zero conductivity in dielectric and flat metal wall, the electric field increases as $|\mathbf{E}| \propto r^{n-1}$, where r is the radial distance to the triple junction point and n follows [18]:

$$\cot n\alpha + \varepsilon_r \cot n(\pi - \alpha) = 0 \quad (4)$$

where α is the angle of vacuum between dielectric and metal and ε_r is the relative electric permittivity of the dielectric.

From eq. (4) it can be concluded that if $\alpha < 90^\circ$ then $n < 1$, leading to infinitely large electric field in the junction, whereas if $\alpha > 90^\circ$ then $n > 1$, leading to null electric field. Only the case with $\alpha = 90^\circ$ leads to $n = 1$, implying a non-zero and non-singular value. However, we are just interested in avoiding singularities, which can be achieved by adjusting $\alpha \geq 90^\circ$. In addition, sharp metallic corners are another source of field singularities which must be avoided.

Regarding the dielectric corners in the junction between the dielectric ring and the iris, it was observed that sharp geometries also lead to field divergences. Thus, the geometry was changed as shown in Fig. 13 and the surface electric field for different round corners was studied for a fine mesh, as illustrated in Fig. 14 and Fig. 15.

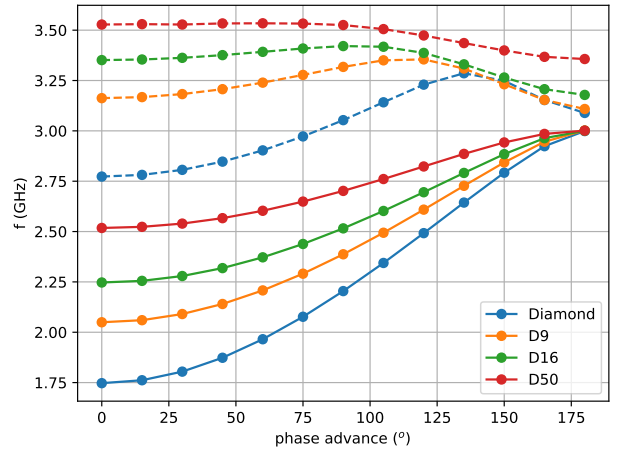
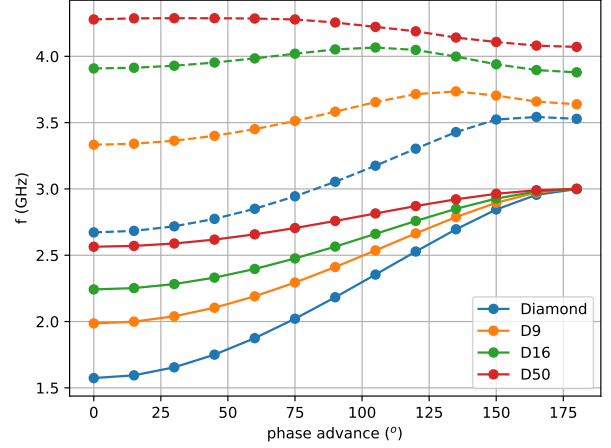


Fig. 12. Dispersion curve of the accelerating mode TM_{02} (solid line) and next higher order mode (dashed line) for different dielectric materials and $\beta = 0.6$ and normalized iris thickness $\xi = 1$ (top figure) and $\xi = 1.5$ (bottom figure).

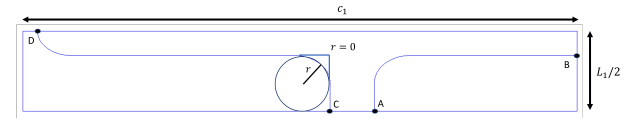


Fig. 13. Geometry modification.

C. Coating effects

Amorphous Carbon (a-C) and Diamond Like Carbon (DLC) coatings were studied at Conseil Européen pour la Recherche Nucléaire (CERN) for Secondary Electron Yield (SEY) reduction in order to avoid multipactor discharges [46]. However, surface losses on the coating, which follow eq. (5), will have an impact on the electromagnetic performance of the cavity

$$P_s = \sigma \int_V |\mathbf{E}|^2 d\tau = \frac{1}{2R} \int |\hat{\mathbf{n}} \times \mathbf{E}|^2 dS, \quad (5)$$

where R is the sheet surface resistance of the coating.

Q_0 as a function of the sheet resistance (in ohms per \square) is illustrated in Fig. 16 for different cases: no coating,

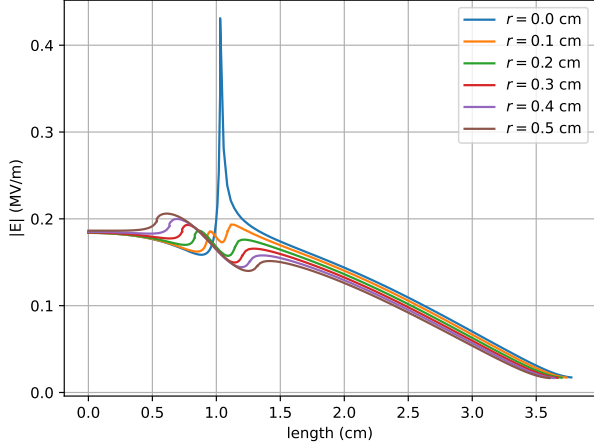


Fig. 14. Electric field magnitude along path AB for different corner radius.

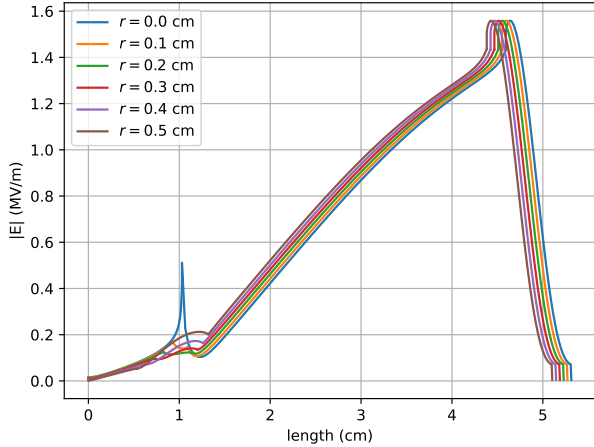


Fig. 15. Electric field magnitude along path CD for different corner radius.

dielectric fully covered with coating, internal coating (which corresponds with coating in region CD) and external coating (which corresponds with coating in region AB). The surface resistance of DLC coating was above $1 \text{ M}\Omega$ per \square and could not be measured, while a-C samples measurements are marked with black dashed lines.

As it can be observed in Fig. 16, Q_0 rapidly decreases for low resistance coatings and therefore thin films or materials with high resistivity are useful coatings to improve the electromagnetic performance.

D. Thermal simulations

In order to estimate the required cooling system and the mechanical stress and deformation induced by RF losses, thermal simulations were carried out using the ANSYS software [47]. Volumetric and surface losses were used as input for steady thermal simulations with 3 cm of copper wall fixing the external temperature at 22°C as boundary condition.

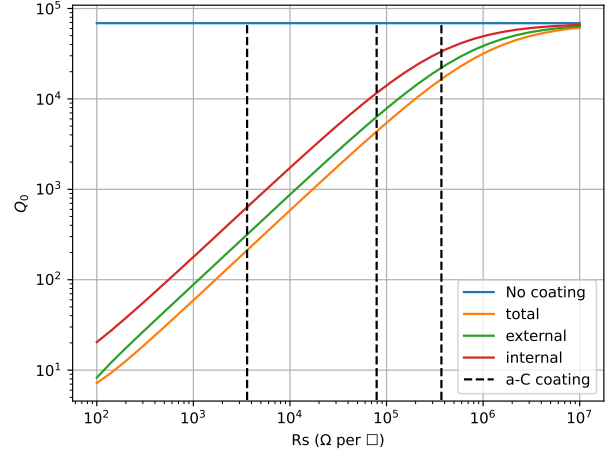


Fig. 16. Comparison of unloaded quality factor of a regular cell partially coated in the external or internal regions of the cavity, full covered and without coating as a function of the sheet resistance.

Simulations were done for different geometries and ceramics, as illustrated in Table II. Ultra high pure alumina was used for simulations instead of MgO because of its higher thermal conductivity in order to evaluate three different meaningful values.

TABLE II
LIST OF DIELECTRICS USED FOR THERMAL SIMULATIONS

Material	ϵ_r	$\tan \delta$	$\kappa \text{ W}\cdot\text{m}^{-1}\cdot\text{K}^{-1}$
CVD Diamond	5.7	3×10^{-6}	2000
Al_2O_3 99.99%	9.8	10^{-5}	30
MgTiO_3	16.66	3.43×10^{-5}	3.8

For numerical simulations, an accelerating gradient of 50 MV/m was used, with a duty cycle $D = 0.075 \times 10^{-3}$,

$$D = \frac{\tau}{T}, \quad (6)$$

where τ is the pulse width and T is the total period of the signal. A graphical solution for Al_2O_3 for $\beta = 1$ is shown in Fig. 17.

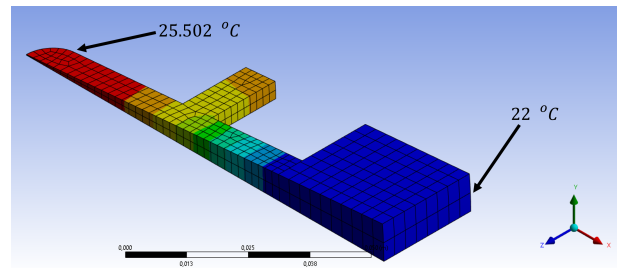


Fig. 17. Steady temperature distribution for Al_2O_3 and $\beta = 1$.

As shown in Fig. 17, the maximum temperature is reached close to the aperture of the ceramic, with a decreasing temperature gradient towards the copper metallic enclosure,

which barely changes thanks to its high thermal conductivity ($\kappa = 400 \text{ W}\cdot\text{m}^{-1}\cdot\text{K}^{-1}$). The maximum temperature reached for different geometries and materials is illustrated in Fig. 18.

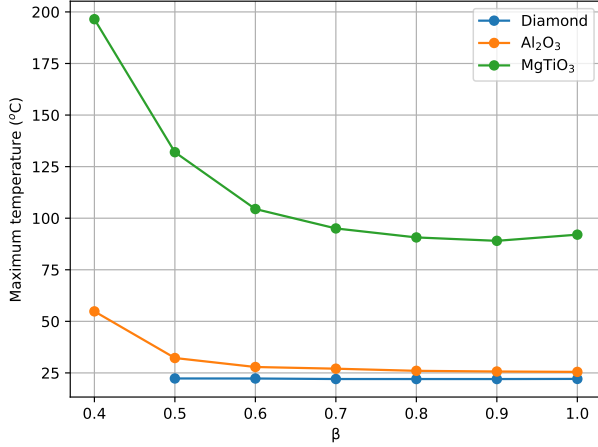


Fig. 18. Maximum temperature reached for different ceramics and particle velocities.

The temperature is higher for lower particle velocity while it seems to saturate at around $\beta = 0.7$ following the behaviour of the Z_{eff} . In addition, very low thermal conductivity, as in MgTiO₃, leads to temperatures beyond acceptable limits regarding stress and deformation tolerances, even though we are still far from the fusion point.

IV. CONCLUSION AND FUTURE WORK

DAA structures for low β particles have been studied for the first time, proving the potential to improve the performance of current room-temperature copper cavities. This study shows improvements in the optimization process and optimal results for an S-band DAA cavity as a solution for compact linear accelerators for Hadrontherapy treatments.

Working under the $\text{TM}_{02-\pi}$ mode, copper ohmic losses can be highly reduced by accumulating electrical energy inside the dielectric. From these studies we could conclude that cavity efficiency increases for higher particle velocity and electric permittivity. However, due to the high energy density inside the dielectric, the cavity performance will be limited by dielectric losses. Therefore, reaching low dielectric loss tangent is a fundamental key in the fabrication of ceramics in particular for DAA cavities.

Iris thickness plays also a fundamental role in the cell optimization by increasing the accelerating voltage and also by reducing the electric energy density inside the ceramic by decreasing dielectric losses. As a consequence, materials with higher loss tangent have thicker optimum irises than ideal geometries.

In addition, the ratio E_p/E_a is lower than those reached by copper cavities, which potentially allows DAA cavities to reach higher gradients without producing RF breakdowns. This ratio decreases for high particle velocity, high electric permittivity and thin irises.

High electric coupling between consecutive cells has been observed for all kind of geometries. In addition, it was shown that coupling improves for lower particle velocity and lower electric permittivity. However low electric permittivity materials, such as CVD diamond, suffer from mode overlapping. In addition, thicker irises produce the excitation of more modes whose resonant frequencies are close to our operational frequency. As a result, the final design must find a compromise between an optimum electromagnetic design, which is achieved for thicker irises and low mode overlapping and low peak electric field, which improve for thinner irises.

Dielectric corners have been rounded in order to smooth the surface electric field. Moreover, stability studies of triple junction point were performed concluding that in order to avoid electric field singularities, the vacuum angle between dielectric and copper must be $\alpha \geq 90^\circ$ and metallic sharp angles must be avoided.

Multipactor is one of the main limitations of DLA cavities due to high SEY of ceramics. Because of that, thin coating with low SEY is used for multipactor suppression. However, surface resistance of coating will have an effect on RF performance that must be studied in advance. Numerical simulations showed that low resistance coatings are unacceptable from an electromagnetic point of view, which implies that only high resistance materials or very thin coatings can be used in order to reduce multipactor.

Finally, thermal conductivity of the ceramic is found to be a crucial parameter also on the design to avoid overheating of the cavity leading to high deformation and stress. Thus, a lower bound value is set around $20\text{-}30 \text{ W}\cdot\text{m}^{-1}\cdot\text{K}^{-1}$ depending on particle velocity and duty cycle.

ACKNOWLEDGMENT

Work supported by Ministerio de Universidades (Gobierno de España) under grant number FPU19/00585 and EST22/00739.

REFERENCES

- [1] T. Shintake, H. Tanaka, T. Hara, T. Tanaka, K. Togawa, M. Yabashi, Y. Otake, Y. Asano, T. Bizen, T. Fukui *et al.*, "A compact free-electron laser for generating coherent radiation in the extreme ultraviolet region," *Nature Photonics*, vol. 2, no. 9, pp. 555–559, 2008.
- [2] E. Tanabe, Y. Fineberg, H. Matsumoto, and T. Shintake, "Medical applications of c-band accelerator technologies," in *Proc. Linear Accel. Conf.*, 1998, pp. 627–629.
- [3] R. Sethi *et al.*, "Electron beam accelerators for materials processing: A bare scnatrion," in *Proc. of APAC*, 2004, pp. 708–710.
- [4] M. Aichele, P. Burrows, M. Draper, T. Garvey, P. Lebrun, K. Peach, N. Phinney, H. Schmickler, D. Schulte, and N. Toge, "A multi-teV linear collider based on clic technology: Clic conceptual design report," SLAC National Accelerator Lab., Menlo Park, CA (United States), Tech. Rep., 2014.
- [5] A. Degiovanni, U. Amaldi, R. Bonomi, M. Garlasché, A. Garonna, S. Verdú-Andrés, and R. Wegner, "Tera high gradient test program of rf cavities for medical linear accelerators," *Nuclear Instruments and Methods in Physics Research Section A: Accelerators, Spectrometers, Detectors and Associated Equipment*, vol. 657, no. 1, pp. 55–58, 2011.
- [6] S. Benedetti, "High-gradient and high-efficiency linear accelerators for hadron therapy," Ph.D. dissertation, Ecole Polytechnique Fédérale de Lausanne, 2018.
- [7] A. Vnuchenko, "High-gradient issues in s-band rf acceleration structure for hadrontherapy accelerators and radio frequency quadrupoles," Ph.D. dissertation, University of Valencia, 2020.

- [8] W. Gai, R. Konecny, and J. Simpson, "Externally powered dielectric loaded waveguides as accelerating structures," in *Proceedings of the 1997 Particle Accelerator Conference (Cat. No. 97CH36167)*, vol. 1. IEEE, 1997, pp. 636–638.
- [9] W. Liu, C. Jing, W. Gai, R. Konecny, and J. Power, "New rf design for 11.4 ghz dielectric loaded accelerator," in *Proceedings of the 2003 Particle Accelerator Conference*, vol. 3. IEEE, 2003, pp. 1810–1812.
- [10] S. Gold, C. Jing, A. Kanareykin, W. Gai, R. Konecny, W. Liu, J. Power, and A. Kinkead, "Development and testing of x-band dielectric-loaded accelerating structures," in *Proc. Part. Accel. Conf.*, 2010, pp. 3001–3003.
- [11] Y. Wei, A. Grudiev, B. Freemire, and C. Jing, "A compact, low-field, broadband matching section for externally powered x-band dielectric-loaded accelerating structures," *IEEE Transactions on Nuclear Science*, vol. 69, no. 5, pp. 991–1001, 2022.
- [12] Y. Wei, H. Bursali, A. Grudiev, B. Freemire, C. Jing, R. Wegner, J. S. Bedolla, and C. Welsch, "Design, fabrication, and low-power rf measurement of an x-band dielectric-loaded accelerating structure," *Physical Review Accelerators and Beams*, vol. 25, no. 4, p. 041301, 2022.
- [13] M. Thompson, H. Badakov, A. Cook, J. Rosenzweig, R. Tikhoplav, G. Travish, I. Blumenfeld, M. Hogan, R. Ischebeck, N. Kirby *et al.*, "Breakdown limits on gigavolt-per-meter electron-beam-driven wakefields in dielectric structures," *Physical review letters*, vol. 100, no. 21, p. 214801, 2008.
- [14] C. Jing, W. Gai, J. Power, R. Konecny, S. H. Gold, W. Liu, and A. K. Kinkead, "High-power rf tests on x-band dielectric-loaded accelerating structures," *IEEE transactions on plasma science*, vol. 33, no. 4, pp. 1155–1160, 2005.
- [15] C. Jing, W. Gai, J. G. Power, R. Konecny, W. Liu, S. H. Gold, A. K. Kinkead, S. G. Tantawi, V. Dolgashev, and A. Kanareykin, "Progress toward externally powered x-band dielectric-loaded accelerating structures," *IEEE transactions on plasma science*, vol. 38, no. 6, pp. 1354–1360, 2010.
- [16] C. Jing, C. Chang, S. Gold, R. Konecny, S. Antipov, P. Schoessow, A. Kanareykin, and W. Gai, "Observation of multipactor suppression in a dielectric-loaded accelerating structure using an applied axial magnetic field," *Applied Physics Letters*, vol. 103, no. 21, p. 213503, 2013.
- [17] C. Jing, S. Gold, R. Fischer, and W. Gai, "Complete multipactor suppression in an x-band dielectric-loaded accelerating structure," *Applied Physics Letters*, vol. 108, no. 19, p. 193501, 2016.
- [18] B. Techaumnat, S. Hamada, and T. Takuma, "Effect of conductivity in triple-junction problems," *Journal of electrostatics*, vol. 56, no. 1, pp. 67–76, 2002.
- [19] B. Freemire, C. Jing, S. Poddar, E. Beamlabs, Y. Zhao, E. Techlabs, M. Conde, D. Doran, G. Ha, W. Liu *et al.*, "High power test of a dielectric disk loaded accelerator for a two beam wakefield accelerator," in *12th International Particle Accelerator Conference (IPAC'21), Campinas, SP, Brazil, 24-28 May 2021*. JACOW Publishing, Geneva, Switzerland, 2021, pp. 1096–1099.
- [20] S. Frankel, "Tm_{0, 1} mode in circular wave guides with two coaxial dielectrics," *Journal of Applied Physics*, vol. 18, no. 7, pp. 650–655, 1947.
- [21] G. Bruck and E. Wicher, "Slow transverse magnetic waves in cylindrical guides," *Journal of Applied Physics*, vol. 18, no. 8, pp. 766–769, 1947.
- [22] A. Oliner, "Remarks on slow waves in cylindrical guides," *Journal of Applied Physics*, vol. 19, no. 1, pp. 109–110, 1948.
- [23] R. S. HARVIE, "A proposed new form of dielectric-loaded wave-guide for linear electron accelerators," *Nature*, vol. 162, no. 4127, pp. 890–890, 1948.
- [24] G. Cohn and G. Flesher, "Design construction and initial operation of a continuous dielectric loaded linear accelerator," *Electron. Res. Laboratories, Illinois Inst. Technol. Chicago, IL, USA, Tech. Rep.*, vol. 2, 1952.
- [25] L. Mullett, W. Walkinshaw, J. Bell, B. Loach *et al.*, "A theoretical and experimental investigation of anisotropic-dielectric-loaded linear electron accelerators," *Proceedings of the IEE-Part B: Radio and Electronic Engineering*, vol. 104, no. 15, pp. 273–290, 1957.
- [26] G. Walker and E. Lewis, "Vacuum breakdown in dielectric-loaded waveguides," *Nature*, vol. 181, no. 4601, pp. 38–39, 1958.
- [27] R. Woode, E. Ivanov, M. Tobar, and D. Blair, "The measurement of the dielectric loss tangent of alumina at microwave frequencies and room temperature," *Electronics Letters*, vol. 30, no. 25, pp. 2120–2122, 1994.
- [28] N. M. Alford and S. J. Penn, "Sintered alumina with low dielectric loss," *Journal of Applied Physics*, vol. 80, no. 10, pp. 5895–5898, 1996.
- [29] C.-L. Huang, J.-J. Wang, and C.-Y. Huang, "Microwave dielectric properties of sintered alumina using nano-scaled powders of α alumina and tio₂," *Journal of the American Ceramic Society*, vol. 90, no. 5, pp. 1487–1493, 2007.
- [30] A. Templeton, X. Wang, S. J. Penn, S. J. Webb, L. F. Cohen, and N. M. Alford, "Microwave dielectric loss of titanium oxide," *Journal of the American Ceramic Society*, vol. 83, no. 1, pp. 95–100, 2000.
- [31] J. D. Breeze, X. Aupi, and N. M. Alford, "Ultralow loss polycrystalline alumina," *Applied physics letters*, vol. 81, no. 26, pp. 5021–5023, 2002.
- [32] A. Kanareykin, "New advanced dielectric materials for accelerator applications," in *AIP Conference Proceedings*, vol. 1299, no. 1. American Institute of Physics, 2010, pp. 286–291.
- [33] C. Jing, A. Kanareykin, S. Kazakov, W. Liu, E. Nenasheva, P. Schoessow, and W. Gai, "Development of a dual-layered dielectric-loaded accelerating structure," *Nuclear Instruments and Methods in Physics Research Section A: Accelerators, Spectrometers, Detectors and Associated Equipment*, vol. 594, no. 2, pp. 132–139, 2008.
- [34] P. Zou, L. Xiao, X. Sun, W. Gai, and T. Wong, "Hybrid dielectric and iris-loaded periodic accelerating structure," *Journal of Applied Physics*, vol. 90, no. 4, pp. 2017–2023, 2001.
- [35] J. Shao, C. Jing, J. Power, M. Conde, and D. Doran, "Study of a dielectric disk structure for short pulse two-beam acceleration," *Group*, vol. 1, no. 10, p. 4, 2018.
- [36] J. Power, W. Gai, S. Gold, A. Kinkead, R. Konecny, C. Jing, W. Liu, and Z. Yusof, "Observation of multipactor in an alumina-based dielectric-loaded accelerating structure," *Physical review letters*, vol. 92, no. 16, p. 164801, 2004.
- [37] C. Jing, A. Kanareykin, J. Power, M. Conde, Z. Yusof, and W. Gai, "Observation of enhanced transformer ratio in collinear wakefield acceleration," in *AIP Conference Proceedings*, vol. 877, no. 1. American Institute of Physics, 2006, pp. 511–519.
- [38] D. Satoh, M. Yoshida, and N. Hayashizaki, "Dielectric assist accelerating structure," *Physical Review Accelerators and Beams*, vol. 19, no. 1, p. 011302, 2016.
- [39] D. Satoh and H. N. Yoshida, M, "Fabrication and cold test of dielectric assist accelerating structure," *Physical Review Accelerators and Beams*, vol. 20, no. 9, p. 091302, 2017.
- [40] S. Mori, M. Yoshida, and D. Satoh, "Multipactor suppression in dielectric-assist accelerating structures via diamondlike carbon coatings," *Physical Review Accelerators and Beams*, vol. 24, no. 2, p. 022001, 2021.
- [41] Y. Wei and A. Grudiev, "Investigations into x-band dielectric assist accelerating structures for future linear accelerators," *IEEE Transactions on Nuclear Science*, vol. 68, no. 5, pp. 1062–1071, 2021.
- [42] K. Halbach and R. F. Holsiger, "Superfish - a computer program for evaluation of rf cavities with cylindrical symmetry," *Particle Accelerators*, vol. 7, pp. 213–222, 1976.
- [43] ANSYS HFSS software. [Online]. Available: <http://www.ansoft.com/products/hf/hfss/>
- [44] V. Bencini, "Design of a novel linear accelerator for carbon ion therapy," Ph.D. dissertation, Rome U., 2020.
- [45] S. Benedetti, A. Grudiev, and A. Latina, "High gradient linac for proton therapy," *Physical Review Accelerators and Beams*, vol. 20, no. 4, p. 040101, 2017.
- [46] A. Grudiev, S. Poddar, H. Neupert, W. Vollenberg, B. Freemire, and C. Jing, "Amorphous and diamond-like carbon coatings for sey reduction of dielectric materials for accelerating structure applications," *Tech. Rep.*, 2022.
- [47] ANSYS software. [Online]. Available: <https://www.ansys.com/>